MULTI-SCALE FAILURE FOR HETEROGENEOUS MATERIALS: LINK WITH MORPHOLOGICAL MODELING – COMPLAS XI

E. Roubin, M. Bogdan and J.B. Colliat

LMT-Cachan
ENS-Cachan, Paris 6 University, CNRS, UniverSud Paris PRES
61 avenue du Président Wilson, 94230 Cachan Cedex, France
e-mail: {roubin,colliat}@lmt.ens-cachan.fr, http://www.lmt.ens-cachan.fr/

Key words: Heterogeneous materials, FE method, Random fields, Excursion set, Embedded discontinuity

Abstract. A 3D meso-scale model for failure of heterogeneous quasi-brittle materials is presented. At such scale, concrete can be represented as an heterogenous material with two phases, where aggregates are included within the concrete. The model problem of heterogeneous materials that is adressed in detail here is based, on the one hand, on FE models with embedded discontinuities and, on the other hand, on a morphological representation using Gaussian or Gaussian related random field excursion sets.

1 Introduction

In view of the growing complexity of macroscopic models of concrete like materials, the question of multi-scale observation became relevant. It clearly appears that macroscopic behaviours of such material (cracking, creep...) take their origin at smaller scales (mesoscopic, microscopic...). The framework presented here is to be seen in this context, and especially in a sequenced way (as opposed to integrated one [1]) where the macroscopic behaviour comes from a mesoscopic description of the material. At this particular scale, concrete must be represented as heterogenous materials. Therefore, both mechanical and geometrical properties have to be represented by the framework.

This communication first present a morphological modeling framework for heterogenous materials. A concrete like material described as a two-phase material is considered here, where inclusions (aggregates) are included within a matrix (cement past and sand). The idea behind this morphological model is to yield the phases from random field excursion sets. Moreover, adding more phases in order to extend possibilities of representation is possible by adding excursion sets. If the framework deals with correlated Gaussian or Gaussian related random field (such as the chi-square distribution - χ^2), an analytic

formulae links the random field characteristics with geometrical and topological quantities (volume, surface area, Euler Characteristic...) of the underlying excursion set. This link has been recently made in [2] giving the possibility of controlling the excursion set characteristics and applying it to represent material phase with chosen characteristics. For a realistic modeling of a concrete like material, both in term of geometrical and topological quantities, due the Gaussian case limitation, an application of the χ^2 random field is made. Both unidimensional Karhunen-Loève decomposition and turning-bands projectional method are used to simulate three dimensional discrete correlated Gaussian random fields.

Efforts of morphological modeling are here made within a multi-scale linear framework using a FE model with embedded discondinuities [3]. In order to represent these heterogeneities, those excursions are projected onto the FE mesh, thus defining a set of discontinuities within the strain field interpolation (weak discontinuities [4]). These kinematics enhancements lead to "non-adapted" meshes in the sense of independence between heterogeneities morphology and the underlying FE mesh. Application of this linear implementation is made for a simple hydration process model presented here.

Considering the non linear failure behaviour, weak discontinuities are completed with a set of strong (displacement field) discontinuities within the framework of local enhancement [5]. Those discontinuities allow for a simple and accurate representation of the meso-scale cracks. The macroscopic response of this model is shown for a simple tension test.

2 Random field generation

As the whole morphological framework is based on Gaussian (or Gaussian related) correlated random field, efforts have to be made in the numerical implementation of their generation. This part explains two methods used to generate realisations of such fields. First the Karhunen-Loève decomposition [6] and then the turning bands projection [7]. Through this paper, we shall call $\gamma(x, w)$ a Gaussian random field over a parameter space M (which shall always be taken here to be a bounded region of $\mathbb{R}^N$) which takes values in $\mathbb{R}$. It is assumed that γ has mean zero, variance σ^2 and is isotropic and stationnary with a Gaussian covariance function defined as $C(x, y) = C(\|x - y\|) = \mathbb{E}\{\gamma(x)\gamma(y)\} = \sigma^2 e^{-\|x-y\|/L_c}$ where L_c is the correlation length.

The orthogonal decomposition of Gaussian correlated random fields theory stipulates [8] that mean zero Gaussian field with continuous covariance function (such as C) can be written as follows

$$\gamma(x, w) = \sum_{n=1}^{\infty} \varphi_n(x)\xi_n(w), \tag{1}$$

where $\xi_n(w)$ are zero mean, unit variance Gaussian random variables, and $\varphi_n(x)$ are functions on M determined by the covariance function C. It is worth noting that eq.(1)

allows for stochastic - w - and spatial -x - variables separation. Therefore, implementing this framework comes to put the effort in the determination of the spatial functions $\varphi_n(x)$.

The Karhunen-Loève decomposition is based on the previous orthogonal decomposition. It allows us to determine these spatial functions $\varphi_n(x)$ for simple compact M in $\mathbb{R}^N$. Demonstration can be found in [9] that they can be determined by first solving the following eigenvalues problem (known as Fredholm problem):

$$\int_M C(x,y)\psi(y)dy = \lambda\psi(x) \tag{2}$$

where λ and ψ are respectively the eigenvalues and eigenvector and then by setting $\varphi_n(x) = \sqrt{\lambda_n}\psi_n(x)$. Theoretically, an infinite sum is needed to define the exact random field in eq.(1). For the numerical implementation made here, a Finite Element Method is used to solve a discretized Fredholm problem. Therefore, using a finite set of eigenvalues and eigenvectors, the following troncated Karhunen-Loève decomposition eq.(3) defines an approximative realization of the underlying random field.

$$\gamma(x,w) = \sum_{n=1}^{m} \sqrt{\lambda_n}\xi_n(w)\psi_n(x). \tag{3}$$

The fact that stochastic and spatial variables are still separated is an essential result for any numerical implementation. Indeed, once the m couples $\{\lambda_n; \psi_n\}$ of a certain correlated random field are determined, the generation of a realization comes to generate a set of independent Gaussian variables (which only requires a random number generator). Moreover, the same couples can be used to produce any other realizations of the same field.

The precision of this method, involving full squared matrix eigenvalues problem, is quickly limitated by the memory storage when one deals with multi-dimensional random fields of large size. The turning bands projectional method has been developped by Matheron [7] in order to reduce the amount of numerical ressources. The idea is to generate several one-dimensional realizations of random fields to produce a multi-dimensional one. The algorithm below explains this projectional method with details.

Let M be the discreted multi-dimensional bounded region where the final realization will be created. Several lines have to be generated (we shall call L their number) with one arbitrary intersection point 0 and an uniform distribution of directions over the unit ball (see Fig.1).

Let $z(\zeta, w_i)$, $i = 1..L$ be the L realizations of a one-dimensional correlated random field generated over the L lines. For each point N on M, the value of the multi-dimensional realization is the average of the one-dimensional realization values at the projection of N on each line i:

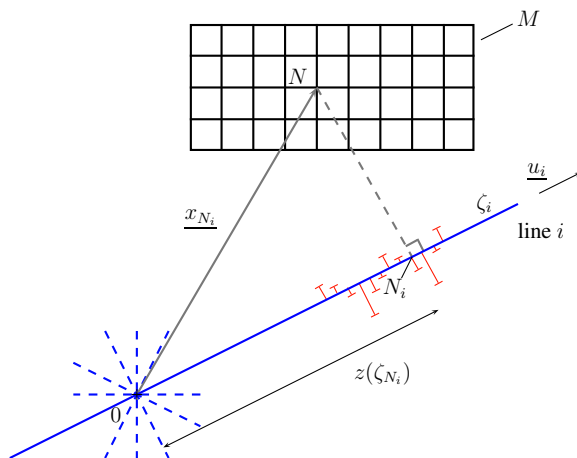$$\gamma(N,w) = \frac{1}{\sqrt{L}} \sum_{i=1}^{L} z(\zeta_{N_i}, w_i) \tag{4}$$

Figure 1: Schematic representation of the turning band method (from [10])

In this paper, the application of the method is made for three-dimensional random fields. The key of this method is the link between the three-dimensional covariance function C and the equivalent one-dimensional covariance function C_1 we need to generate the L realizations. Let $C(r)$ be as above (with $r = \|x - y\|$). Following [7] we have

$$C_1(r) = \frac{d}{dr}(rC(r)) = \sigma^2\left(1 - \frac{2r^2}{L_c^2}\right)e^{-r^2/L_c^2} \tag{5}$$

3 Excursion Set

We call an excursion set the morphology of a subset of a bounded region defined by thresholding a realization of a random field. It allows us to create a set of random shapes. Let γ be a realization of $\gamma(x, w) : M \subset \mathbb{R}^N \to \mathbb{R}$ define as above and $u \in \mathbb{R}$ a chosen threshold. The underlying excursion set A_u is defined by the points of M where the values of γ are above u (eq.(6)).

$$A_u \equiv A_u(\gamma, M) \triangleq \{x \in M : \gamma(x) \geq u\} \tag{6}$$

This principle, applied for $M \in \mathbb{R}$ is shown on Fig.2.

In our case, random fields will be yield in a three dimensional space ($M \subset \mathbb{R}^3$) and therefore define three-dimensional excursion sets. The two excursions represented in Fig.3 are made from the same realization with two different threshold values. It is clear that, by changing this value, a large range of varied morphologies can be generated. This exemple shows that "low" values of u produce excursions mainly made of handles with high volume fraction, giving a "sponge" like topology (Fig.3(a)), whereas "high" values of u produce excursion made of several connected components with a lower volume fraction (Fig.3(b)).

In order to provide a global description of the resulting morphology, the Lipschitz-Killing curvatures, hereafter LKCs, are choosen. In a N-dimensional space $N + 1$ LKCs can be defined where each can be thought of measures of the "j-dimensional sizes" of
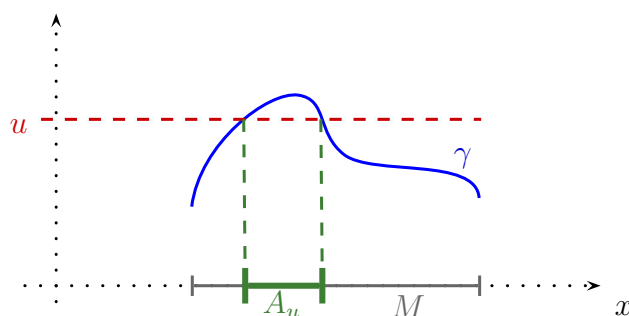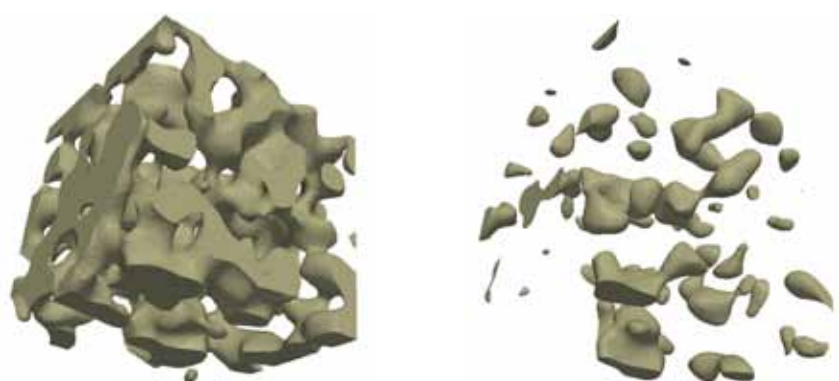
Figure 2: Schematic representation of a one-dimensional excursion set A_u

(a) "Low" threshold - sponge topology

(b) "High" threshold - meatball topology

Figure 3: Effect of threshold value on tri-dimensional excursion topology

A_u. In our three-dimensional case, the four LKCs, denoted by $\mathcal{L}_j$, $j = 0..3$, provide both geometrical - $\mathcal{L}_1$, $\mathcal{L}_2$, $\mathcal{L}_3$ - and topological - $\mathcal{L}_0$ - descriptions of the morphology A_u. They are defined by:

- $\mathcal{L}_3(A_u)$ is the three dimensional volume of A_u.

- $\mathcal{L}_2(A_u)$ is half the surface area of A_u.

- $\mathcal{L}_1(A_u)$ is twice the caliper diameter of A_u.

- $\mathcal{L}_0(A_u)$ is the Euler characteristic of A_u, which contrary to the other LKCs is a topological measure. In three-dimension, it can be calculated by:

  $\mathcal{L}_0(A_u) = \#\{\text{connected components in } A_u\} - \#\{\text{"handles" in } A_u\} + \#\{\text{"holes" in } A_u\}$

  For exemple, a ball or a cube are topologicaly identical (Euler characteristic $\mathcal{L}_0 = 1$) but differ from a hollow ball ($\mathcal{L}_0 = 2$) or a ring torus ($\mathcal{L}_0 = 0$).

Following [2], a probabilistic link has been made between excursion set properties and random field thresholding parameters giving an explicit formulae for the expectation of the LKCs - $\mathbb{E}\left\{\mathcal{L}_i\left(A_u\left(\gamma, M\right)\right)\right\}$. It is not the purpose of this paper to give details on these formulae, however, full proof and details can be found in [9]. The only idea one need to remember to go through this paper is that this theory gives a new tool helping us to predict all the geometrical and topological properties of an excursion set from the random field characteristics and the threshold - σ, L_c, u -. These relations have been made explicit for $\gamma(x, w)$ as above on a cube $M = \prod_{i=1}^3 [0; T]$:

$$
\begin{cases}
\mathbb{E}\{\mathcal{L}_0\}(A_u) &= \left(\frac{\sqrt{2}}{2\pi^2}\frac{T^3}{L_c^3}\left(\frac{u^2}{\sigma^2}-1\right) + \frac{3\sqrt{2}}{2\pi^{3/2}}\frac{T^2}{L_c^2}\frac{u}{\sigma} + \frac{3\sqrt{2}}{2\pi}\frac{T}{L_c}\right)e^{-u^2/2L_c^2} + \Psi\left(\frac{u}{\sigma}\right) \\
\mathbb{E}\{\mathcal{L}_1\}(A_u) &= \left(\frac{\sqrt{2}}{\pi^{3/2}}\frac{T^3}{L_c^2}\frac{u}{\sigma} + \frac{3\sqrt{2}}{4}\frac{T^2}{L_c}\right)e^{-u^2/2L_c^2} + 3T\Psi\left(\frac{u}{\sigma}\right) \\
\mathbb{E}\{\mathcal{L}_2\}(A_u) &= \frac{\sqrt{2}}{\pi}\frac{T^3}{L_c}e^{-u^2/2L_c^2} + 3T^2\Psi\left(\frac{u}{\sigma}\right) \\
\mathbb{E}\{\mathcal{L}_3\}(A_u) &= T^3\Psi\left(\frac{u}{\sigma}\right)
\end{cases}
\tag{7}
$$

Fig.4(a) and Fig.4(b) represent respectively the Euler characteristic and the volume fraction - directly linked with the fourth LKC by $\mathbb{E}\{\mathcal{L}_3\}(A_u)/T^3$ - of excursion sets of $\gamma(x, w)$ for u from -20 to 20.
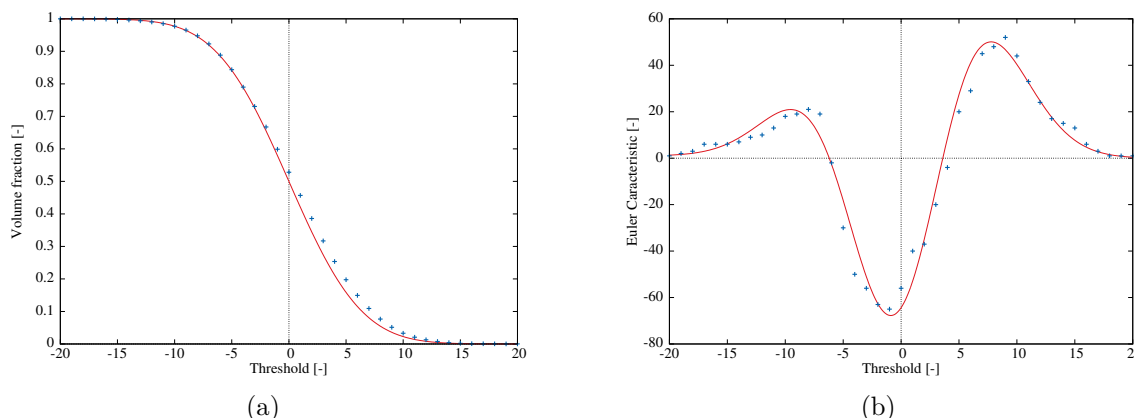

(a)

(b)

Figure 4: LKCs of excursion sets of Gaussian random field in term of threshold values.

—— Expected values of LKCs provided by (7), + Numerical values calculated from one realization of $\gamma(x, w)$.

The constant decreasing shape of the volume fraction curve in term of u clearly reflects the effect of the threshold level on the "size" of A_u. Even if more peculiar, the Euler characteristic curve shape reflects also easily the effect of the threshold on excursion sets topology. For values of u lower than the lowest value of γ, the Euler characteristic is the one of the full cube ($\mathcal{L}_0 = 1$). By increasing u, several holes appear, counting in positive for the Euler characteristic ($\mathcal{L}_0 > 1$). Then, the expansion of the holes starts to form handles which lead to a sponge like topology ($\mathcal{L}_0 < 0$). By increasing u even more,

handles disappear forming a "meatball" like topology of connected components ($\mathcal{L}_0 > 0$). Finally, the Euler characteristic decreases to $\mathcal{L}_0 = 0$ when no more connected components remain.

From the comparison between theorical values and measures on one realization, we can point out that the variability of the numerical generation is very low. Therefore, although eq.(7) gives only expectations of LKCs, for this range of excursion sets we can assume that $\mathbb{V}\{\mathcal{L}_i(A_u)\} \ll 1$.

So far, we have seen the effect of the threshold value on excursion sets. But one needs to remember that, according to eq.(7), both variance and covariance length of $\gamma(x, w)$ affect the morphology as well. Understanding the full behaviour of these equations is a key point for anyone who wants to make excursion set modeling.

4 Application of the modeling framework on concrete like material

The material is represented as an heterogeneous material with two phases. One phase (aggregates) is represented by an excursion set of a correlated random field while its second phase (concrete) is represented by its complementary. Therefore in this part, the effort will be put in a "realistic" representation of the aggregates phase. We keep only three relevant characteristics from the four LKCs: the volume fraction V_v, the volumic surface area $\mathcal{S}$ and the number of agregates $\mathcal{N}$ which are respetively linked with $\mathcal{L}_3$, $\mathcal{L}_2$ and $\mathcal{L}_0$. Thought V_v and $\mathcal{S}$ can be directly estimated, attention must be taken when it comes to $\mathcal{N}$. Indeed the Euler characteristic does not indicate the number of aggregates for every topology. In our case, the "meatball" topology has to be targeted and it is only once we assume that the excursion set is free from holes and handles that $\mathcal{N}$ can be estimated by $\mathcal{L}_0$. In this specific kind of topology: $\mathcal{N} \triangleq \#\{\text{connected components}\} = \mathcal{L}_0$.

Once the three characteristics $(\mathcal{N}, \mathcal{S}, V_v)$ of the phase are set, the generation of the underlying excursion set rely on finding a solution for (u, σ, L_c) that satisfy the following system:

$$\begin{cases} \mathbb{E}\{\mathcal{L}_3\}(u, \sigma) & = V_v T^3 \\ \mathbb{E}\{\mathcal{L}_2\}(u, \sigma, L_c) & = \frac{1}{2}\mathcal{S}T^3 \\ \mathbb{E}\{\mathcal{L}_0\}(u, \sigma, L_c) & = \mathcal{N} \end{cases} \tag{8}$$

Due to the intrinsic non linearity of eq.(7), depending on the different values of $(\mathcal{N}, \mathcal{S}, V_v)$ (especially for "meatball" topology - $\mathcal{N} \gg 1$) the problem eq.(8) do not always have a solution. For exemple, we can clearly see on Fig.4 that we can not expect $\mathcal{N}$ to be upper than 40 while keeping a "high" volume fraction ($V_v > 40\%$). Which in our case of concrete like material modeling leads to a major issue. So far, the more realistic solution for "meatball" topology we get with this framework allows us to represent an aggregate phase with a maximum of 15% volume fraction.

Until now, the framewok has been presented considering Gaussian random fields. But estimation of LKCs for excursion set can also be worked out considering Gaussian related fields. The application of this paper is made using a chi-square distribution with k degrees

of freedom - χ_k^2 -. Realizations of such fields can be seen as sum of k independent squared realizations of a correlated Gaussian random field. Let δ be a realization of such field and γ_i, $i = 1..k$ be k realizations of the Gaussian field $\gamma(x, w)$ described above. We have :

$$\delta = \sum_{i=1}^{k} \gamma_i^2 \tag{9}$$

Although similar to eq.(7), the use of a χ_k^2 distribution add the parameter k to the system eq.(8). With such field, the nearest solution is found for $k = 1$ and enable us to double the previous volume fraction $V_{v_{max}} \approx 30\%$. Fig.5 shows a two-dimensional slice of excursions from a Gaussian realization and a χ_1^2 made from the same realization. Fig.5(b), being the excursion from the squared realization of the excursion Fig.5(a), shows clearly that, for the same threshold, it is natural to expect the volume fraction to double between excursions of Gaussian and χ_1^2 random fields.
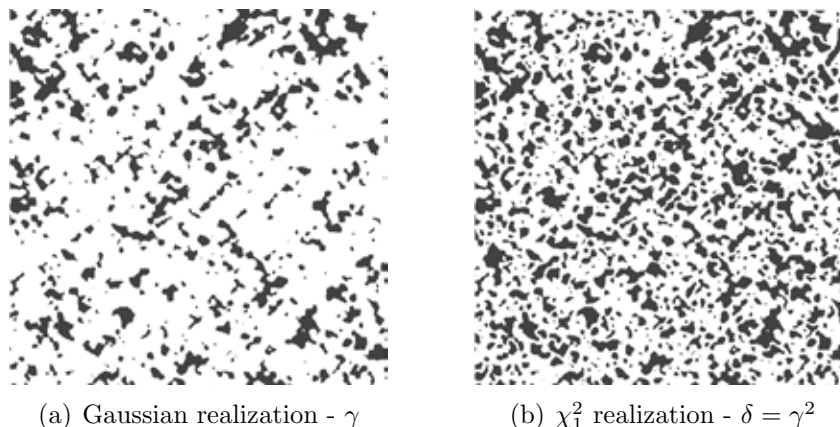

(a) Gaussian realization - γ (b) χ_1^2 realization - $\delta = \gamma^2$

Figure 5: Comparison between Gaussian and χ_1^2 excursion sets for the same threshold value.

The χ_1^2 distribution remains the more suitable solution for meatball topology and high volume fraction morphology we found.

5 FE model for heterogeneous material - Application to hydration process modeling

The approach made here relies on a spatial truss, to model pattern of heterogeneities. The choice of a not adapted meshing process is made here thus, the spatial positions of nodes are not constrained by the morphology. Therefore, both gemetrical and mechanical properties have to be handle inside some interface elements. These cut elements are split into two parts, each having different elastic properties by enhancing them with strain (weak) discontinuities [11]. An elementary enhancements method (E-FEM) method for kinematic enhancement of Finite Element using the Hu-Washizu variational formulation is used here. For example, if we consider a two-phase material (inclusions within a matrix),

three sets of elements are needed: those entirely in the matrix, those entirely in the inclusions, and those which are split between both (cut elements). To calculate these elements repartition, a projection of the previous excursion set is made onto the truss. In order to illustrate this linear framework, a simple hydration process of concrete like material modeling has been implemented. Considering a simplistic version of the Powers and Brownyard hydration model [12], with only three phases: unreacted cement, hydration products (including gel water) and free water, the volume fraction of each one of them can be calculated according to the following equations:

$$
\begin{cases}
p = \frac{w/c}{w/c + \rho_w/\rho_c} \\
V_{anh} = (1-p)(1-\alpha) \\
V_h = 2.12(1-p)\alpha \\
V_w = 1 - V_h - V_{anh}
\end{cases}
\tag{10}
$$

where p is the initial porosity, α the hydration degree and V_{anh}, V_h, V_w respectively the volume fractions of anhydrous cement, hydration products and water.

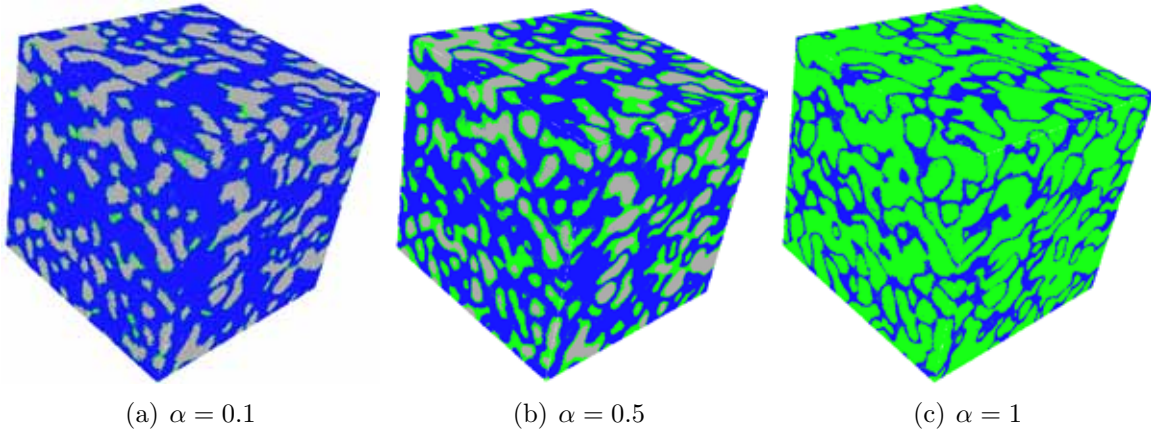(a) $\alpha = 0.1$ (b) $\alpha = 0.5$ (c) $\alpha = 1$

Figure 6: Projection of excusion set shapes on FE truss for different hydration degrees.

■ water, ■ hydration products, ■ anydrous cement

As explained previously, thresholding a random field with a scalar allows to create a two phase material. One can easily imagine, that a second threshold, with a different value, will allow to create an additional phase, concentrical to the first one. Therefore, setting two thresholds will allow us to create a three phase material. Thus, for different hydration degrees, each phase's volume fraction is known and can be linked to the random field's thresholds u_i (equation eq.(7)). Eventually, the initial morphology is set up by one threshold (two phases: water and unhydrated cement), and then, for a growing hydration degree, two thresholds are calculated and applied to the random field, creating a three phase material (water, unhydrated cement and hydration products).

Within this framework, macroscopic material characteristics like Young modulus can be estimated over a given hydration degree with simple tension tests. The following

characteristics have been chosen $E_{anh} = 135\,000\ MPa$, $E_h = 25\,000\ MPa$ and $E_w = 1\ MPa$.
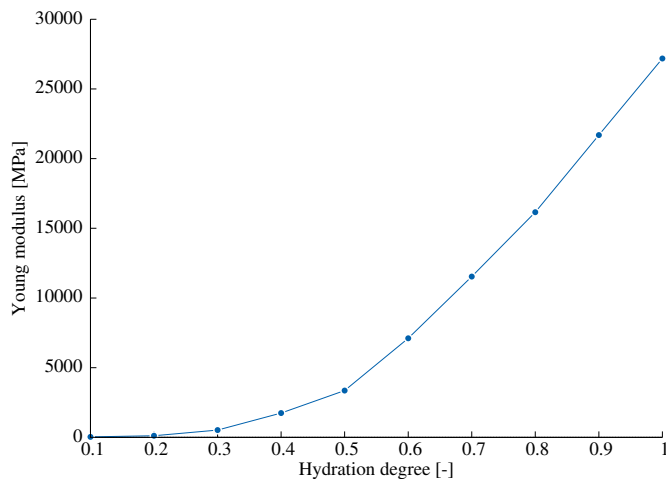

Figure 7: Young modulus of a concrete like material for different hydration degrees.

Fig.7 shows that the continuous growing of the macroscopic Young modulus over hydration degree is well handled by this FE representation. A slight raising of the slope can be seen after $\alpha = 0.4$.

6 FE models with embedded discontinuities

In addition to the geometrical representation of heterogeneities, displacement (strong) discontinuities are also introduced in the elements, in order to model a non-linear softening response based on failure quasi-brittle. These discontinuities represent micro-cracks that can occurs in both phases as well as at the interfaces (debonding). Details of this FE numerical implementation can be found in [3].

A other simple tension test is presented here. Material properties are defined according to Tab.1.

Table 1: Material properties

Matrix	Inclusions	Interface
$E = 10 GPa$	$70 GPa$	$-$
$\sigma_u = 3 MPa$	$-$	$3 MPa$
$Gf = 11 J/m^2$	$-$	$11 J/m^2$

Two remarks are worthy of attention. The first is that the interface is of rigid-brittle type. The second is that we choosed for inclusions to remains in the linear elastic regime.
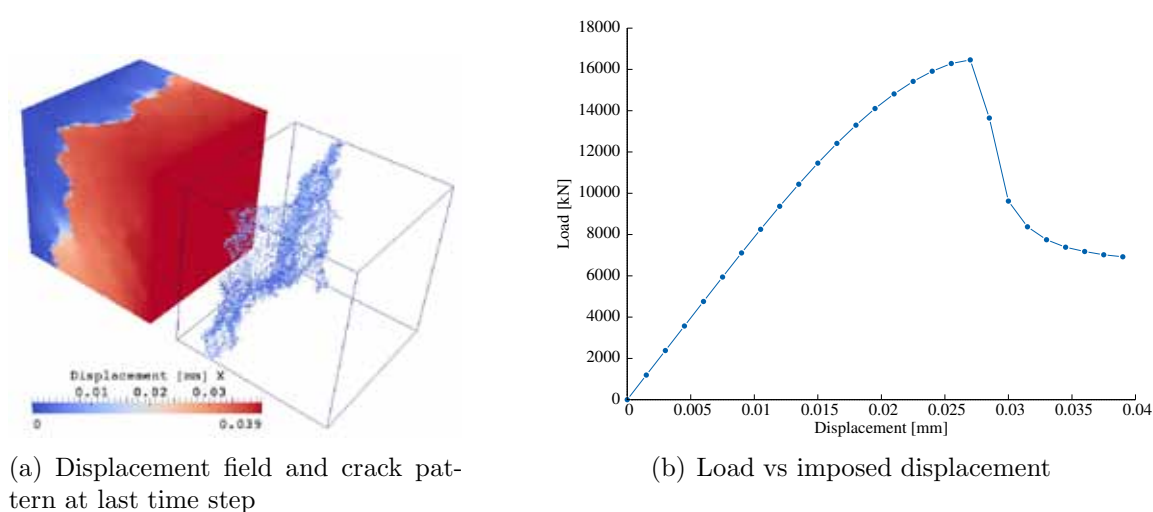
(a) Displacement field and crack pattern at last time step

(b) Load vs imposed displacement

Figure 8: Results for simple tension

The cracking pattern is shown on Fig.8(a) where two zones are splited by a macroscopic crack (represented by means of the broken elements). Fig.8(b) shows the macroscopic load vs imposed displacement curve where three steps can be seen. First, a linear part where no failure occurs. Then, with the apparition of several microscopic cracks, we can observe a yield behaviour. Finaly, the softening part begin when the localisation of these microscopic cracks creates a macrosopic one.

7 Concluding remarks

This communication presents a first attempt to create a sequential multi-scale framework where morphology of heterogeneous material is defined by excursion sets of correlated random fields. Though, efforts still have to be made in order to generate more realistic morphologies, advantages have been shown through two examples. We can also add that this framework is well adapted to other problematics related with concrete like materials such as the effect of morphological variability on macroscopic behaviour. Indeed, the use of both Karhunen-Loève decomposition and non-adapted meshes allows fast computations, limiting the growing amount of numerical ressources needed when dealing with large sets of morphologies. Futhermore, being able to represent broken elements by means of a strong discontinuity in the FE method allows calculations of permeability or diffusion in such damaged materials [13].

REFERENCES

[1] Feyel, F. and Chaboche, J.-L. Multi-scale non-linear FE analysis of composite structure: damage and fiber size effects. *Revue européenne des Éléments Finis : NUM-DAM'00 isues* (2001) **10**:449–472

[2] Adler, R.J. Some new random field tools for spatial analysis. *Stochastic Environmental Research and Risk Assessment* (2008) **22**:809–822

[3] Benkemoun, N., Hautefeuille, M., Colliat, J.-B., Ibrahimbegovic, A. Failure of heterogeneous materials: 3D meso-scale FR models with embedded discontinuities. *Int J. Num. Meth. in Engng.* (2010) **82**:1671–1688

[4] Sukumar, N., Chapp, D.L., Moës, N. and Belytshcko, T. Modeling holes and inclusions by level sets in the extended finite element method. *Computer Methods in Applied Mechanics and Engineering* (2001) **190**:6183–6200

[5] Oliver J. Modelling strong discontinuities in solid mechanics via strain softening constitutive equations. *International Journal for Numerical Methods in Engineering* (1996) **39**:3575–3623

[6] Loeve, M. Probability Theory. *Graduated Texts in Mathematics* (1978) Vol. II, 4th ed..

[7] Matheron, G. The intrinsic random functions and their applications. *Advances in Applied Probability* (1973) **5**:439–468

[8] Karhunen, K. Über lineare Methoden in der Wahrscheinlichkeitsrechnung. *Ann. Acad. Sci. Fennicae. Ser. A. I. Math.-Phys* (1947) **37**:1–79

[9] Adler, R.J. and Taylor, J.E. *Random Fields and Geometry* (2007) Springer, Boston

[10] Mantoglou, A. and Wilson, J.L The Turning Bands Method for Simulation of Random Fields using Line Generation with a Spectral Method *Water Resources Research* (1982) Vol.II, **2**:129–149

[11] Ortiz, M., Leroy, Y. and Needleman, A. A Finite Element method for localized failure analysis *Computer Methods in Applied Mechanics and Enginnering* (1987) **61**:189–214

[12] Powers, T.C. and Brownyard, T.L. Studies of the physical properties of hardened Portland cement paste. *J. Am. Concr. Inst.*, (1947). **43**101–132, 249–336, 469–505, 549–602, 669–712, 845–880, 933–992.

[13] Jourdain, X., Colliat, J.-B., De Sa, C., Benboudjema, F. and Gatuingt, F. Upscaling permeability for fractured concrete : meso-macro numerical approach within a sequential framework *submitted*